Acta Materialia 191 (2020) 245–252

Contents lists available at ScienceDirect

Acta Materialia

journal homepage: www.elsevier.com/locate/actamat

Full length article

Thickness Dependence of crack initiation and propagation in stacks for piezoelectric microelectromechanical systems

Kathleen Coleman[a,b,*], Raul Bermejo[b,c], Dominique Leguillon[d], Susan Trolier-McKinstry[a,b]

[a] Materials Research Institute, Pennsylvania State University, Univesrity Park, PA, USA
[b] Materials Scienc and Engnineergin Department, Pennsylvania State University, Uivesrity Park, PA, USA
[c] Department of Materials Science, Montanuniversitaet Leoben, Austria
[d] Institut Jean Le Rond d'Alembert – CNRS, Sorbonne Université, Paris, France

ARTICLE INFO

Article History:
Received 7 October 2019
Revised 18 March 2020
Accepted 19 March 2020
Available online 9 April 2020

Keywords:
Piezoelectricity
Mechanical behavior
Microelectromechanical systems
Thin films
Fracture stress

ABSTRACT

Piezoelectric thin films are vulnerable to fracture, which results in degradation of the structural integrity and device performance in piezoelectric microelectromechanical systems (PiezoMEMS). This work explains the fracture process as a combination of a crack initiation event in the piezoelectric film followed by crack propagation through the remaining layers. Biaxial bending tests using the Ball-on-three-Balls (B3B) technique were performed on stacks containing $Pb(Zr_{0.52}Ti_{0.48})O_3$ (PZT) thin films of varying thicknesses grown on Si wafers (coated with thin $LaNiO_3/SiO_2$ layers). The fracture initiates in the PZT film, arrests in the compressive SiO_2 layer, prior to failure of the Si substrate. Weibull analyses show a significant effect of the thin film thickness on the stack's strength; the characteristic strength and Weibull modulus being σ_0 ~1110 MPa and m ~28, σ_0 ~1060 MPa and m ~26, and σ_0 ~880 MPa and m ~10 for the 0.7 μm, 1.3 μm, and 1.8 μm film stack, respectively and σ_0 ~ 1820 MPa and m ~3 for the Si wafer. A stress-energy criterion using finite fracture mechanics explains the dependence of crack initiation load on the PZT layer thickness, whereas linear elastic fracture mechanics is employed to rationalize crack propagation through the stack.

1. Introduction

Piezoelectric microelectromechanical systems (piezoMEMS) are utilized in sensors, transducers, actuators, and energy harvesting devices [1,2]. These devices contain multilayer stacks composed of active piezoelectric layers and their electrodes, with additional layers for adhesion and support. Materials with high piezoelectric coefficients, such as lead zirconate titanate with a morphotropic phase boundary composition of $Pb(Zr_{0.52}Ti_{0.48})O_3$ (PZT) [1–3] are typically used in order to provide high sensitivity sensors or large displacement actuators. PiezoMEMS devices contain thin piezoelectric layers (typically between 0.3 and 3 μm in thickness) [4–6], which enable significant reduction in the voltage required to reach target electrical fields, relative to bulk ceramics or single crystals. The thickness of the piezoelectric layer is optimized to enhance the piezoelectric response and functionality of the device. For example, thinner films are used for lower voltage applications, while increasing the thickness of the piezoelectric layer can yield a higher power density for energy harvesting devices, due to the increase in the active volume [4]. In addition, thicker films tend to be less clamped to the substrate which allows for more domain wall mobility, which may enhance their piezoelectric response [5,6]. However, thick films are commonly observed to crack under smaller applied strains than thinner films. Therefore, it is mandatory to understand the relationship between the thin film's thickness and the structural integrity of the stack to properly design piezoMEMS.

Piezoelectric films layers grown via sputtering or chemical solution deposition are typically under significant residual stress. In chemical solution deposition, the residual stress is due primarily to the thermal expansion coefficient mismatch between layers [7–12], with partial relief of the stress possible due to either bending or to the domain structure in ferroelectric layers [9,10,13–15]. The residual stresses affect the film's domain structure and piezoelectric response [8,16,17] and may also lower the electrical breakdown strength [18]. Films experience further mechanical stresses from bending (e.g. in energy harvesters and sensors) and the piezoelectric effect (under an applied electric field) during use. As a result, failure of piezoMEMS stacks can occur in response to a combination of electrical and mechanical loading [18–21]. Electrical failure often results in a series of thermal breakdown events connected through cracks [19].

Prediction of cracking in these systems is very challenging, as the microstructure, domain structure [22–25], orientation, grain size, and surface quality may influence the mechanical response of the

* Corresponding author at: Materials Research Institute, Pennsylvania State University, N225 Millenium Science Complex, University Park, PA 16802, USA.
E-mail address: kpc8@psu.edu (K. Coleman).

https://doi.org/10.1016/j.actamat.2020.03.030
1359-6454/

brittle film [24,26–29]. Additionally, adhesion between layers, interfaces properties, and surface condition (e.g. polish, etch, etc.) may also affect the structural integrity of the multilayer stack [27]. It has been observed that the thickness of the piezoelectric layer affects the structural integrity of the entire stack; stacks with thicker layers are more prone to cracking than stacks with thinner films [18]. Previous studies suggest that the stress required for crack initiation can be a function of thickness either due to a volume effect in Weibullian materials [30] or differences in the residual stress as a function of thickness [10,31]. To date, the underlying mechanism for crack initiation in PiezoMEMS is not well understood. Models based on fracture mechanics suggest that the film thickness will affect the conditions for crack initiation in the films. Because crack initiation is contingent on the strain energy accumulated in the film during mechanical loading, it is harder to initiate cracks when the layers are thin [32].

This paper investigates the relationship between PZT film's thickness and the fracture response of the stack under mechanical loading. PZT/$LaNiO_3$/SiO_2/Si stacks with different PZT thickness were tested in biaxial loading conditions. Strength distributions of the different stacks were evaluated using Weibull statistics and compared to SiO_2/Si samples as a reference. The effect of PZT thickness on crack initiation was investigated in samples pre-loaded below the stack failure strength. Models for crack initiation and for crack propagation were derived based on fracture mechanics considerations. This study can be used to set structural limits on achievable strains in piezoMEMS.

2. Experimental Procedure

Double-side polished 4″ Si wafers with a 1 μm thick thermal SiO_2 layer on both surfaces were obtained from Nova Electronic Materials. A 150 nm layer of $LaNiO_3$ (LNO) was deposited on one surface using an acetic acid based solution, as reported elsewhere [17,33]. This layer acts both as a template for {001} orientation of the perovskite structure and as a bottom electrode. Then, {001} oriented $Pb_{0.99}\square_{0.01}(Zr_{0.52}Ti_{0.48})_{0.98}Nb_{0.02}O_3$ films of 0.7 μm, 1.3 μm, and 1.8 μm were grown by chemical solution deposition (CSD) using a 2-methoxyethanol based solution (Fig. 1a) [17,34,35]. The orientation and phase purity of the films were characterized by a Merlin field-emission scanning electron microscope (FeSEM) and by X-Ray Diffraction (XRD) using a PANalytical Empyrean with a Cu K_α X-Ray source to calculate the Lotgering factor. PZT/$LaNiO_3$/SiO_2/Si stacks with different PZT thickness, i.e. 0.7 μm, 1.3 μm and 1.8 μm, were diced into 12 × 12 mm squares and tested in biaxial loading conditions (Fig. 1b). Reference samples of the Si substrate with a 1 μm SiO_2 layer were also tested for comparison.

The ball on three balls (B3B) biaxial test method was used to determine (i) the strength distribution of the different samples and (ii) the conditions for crack initiation in the PZT films [36,37]. In this loading configuration, the rectangular plates are symmetrically supported by three balls on one face and loaded by a fourth ball in the center of the opposite face (see Fig. 1b); this guarantees well-defined three-point contacts. The four balls had a diameter of 7.5 mm, giving a support diameter of 8.65 mm. At the midpoint of the plate surface, opposite to the loading ball, a biaxial tensile stress is generated. One of the main advantages of this method is that the maximal stress developed during the test is located far from the edges (corners) of the sample, i.e. away from edge defects [36,38–40]. A total of 20 specimens per sample were tested to failure using a universal tester (Instron, Ma). A pre-load of ~10 N was employed to hold the specimen between the four balls. Tests were conducted under displacement control of 0.1 mm/min in ambient conditions (~22 °C and ~40% RH). The stress at the surface under tension was calculated according to Eq. (1) [36]:

$$\sigma_f = f * \frac{F}{t^2} \tag{1}$$

where F is the applied force, t is the thickness of the stack, and f is a geometry factor, which depends on the diameter of the balls, thickness of the sample, and Poisson's ratio, ν, of the material. The factor f was calculated using finite element analysis, resulting in f = 2.4 for t = 0.502 mm and ν = 0.3. The failure stress (σ_f) was calculated assuming a homogeneous Si sample. The stresses in the PZT, LNO, and SiO_2 layers were calculated assuming the strain on the top of the Si is equal to the strain in these thin layers, as described in the supplemental material section. A Weibull statistical analysis was performed according to the ASTM standards [31,41].

To investigate crack initiation, selected specimens were loaded between 20% and 80% of the characteristic Weibull stress of the different samples (load increments of 5%). Each of these samples was

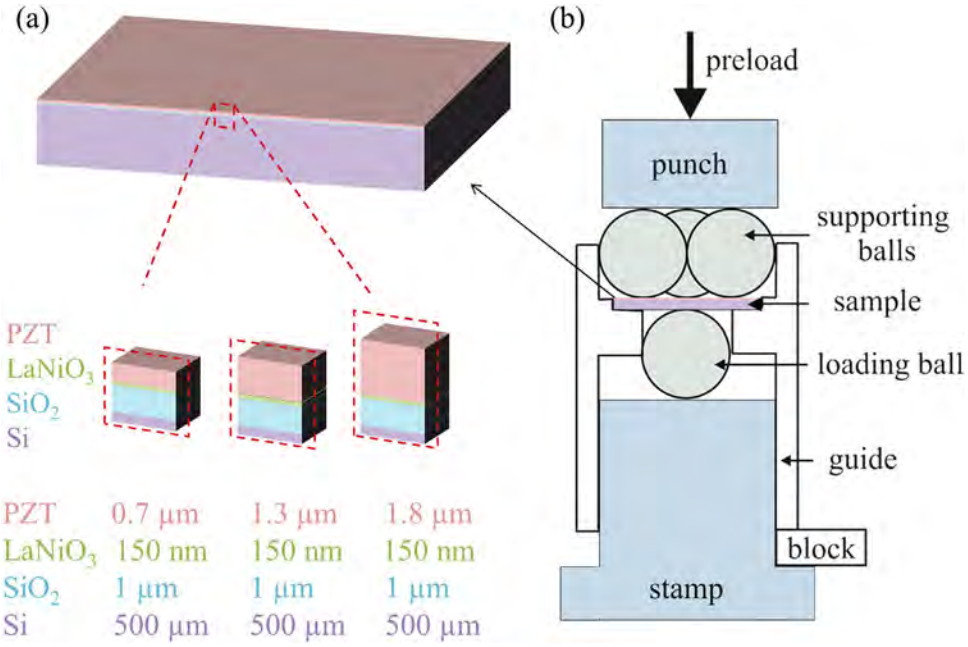

Fig. 1. Schematic of the samples where PZT of varying thicknesses is grown on top of Si wafer (a), and a schematic of the ball on three balls test setup (b).

only loaded once. The PZT side of the stack was then imaged using an oversaturated dark field optical microscope to assess the presence of cracks. The lowest load at which cracking was observed was recorded as the stress required for crack initiation in the PZT layer. In order to determine the depth of the surface pre-cracks, a FEI Scios Focus Ion Beam (FIB) was employed. Cross-sections were made from the top PZT surface down to the SiO_2 layer. From these results, crack initiation and propagation models were developed.

3. Results

3.1. Microstructure

Fig. 2 shows the FESEM and XRD patterns for the different samples. All PZT films had strong {100} orientation, with comparable Lotgering factors of 99%, 97% and 99% for the 0.7 μm, 1.3 μm, and 1.8 μm PZT films, respectively. The average surface grain size of the 0.7 μm, 1.3 μm, and 1.8 μm PZT film is 86 $\pm$ 7 nm, 105$\pm$ 20 nm and 106 $\pm$ 14 nm, respectively. All of these grain sizes fall within the first standard deviation of each other.

3.2. Strength distribution

Fig. 3 shows the strength distribution of the different sample sets represented as a Weibull diagram; the corresponding characteristic strength, σ_0, and Weibull moduli, m, are also tabulated in Table 1 along with the 90% confidence intervals. It is apparent that the SiO_2/Si/SiO_2 substrates have the highest characteristic strength (σ_0 = 1815 MPa) and the lowest Weibull modulus ($m \sim 3$). Si substrates tend to have a broad population of critical flaw sizes [27–29,39,42,43], which is consistent with the low Weibull modulus observed in this study. The Weibull strength decreases with the addition of the thin PZT/$LaNiO_3$ layers. That is, the PZT layer reduces the strength of the stack [38,39]. It is also apparent that stacks with thinner PZT layers have higher characteristic strength than stacks

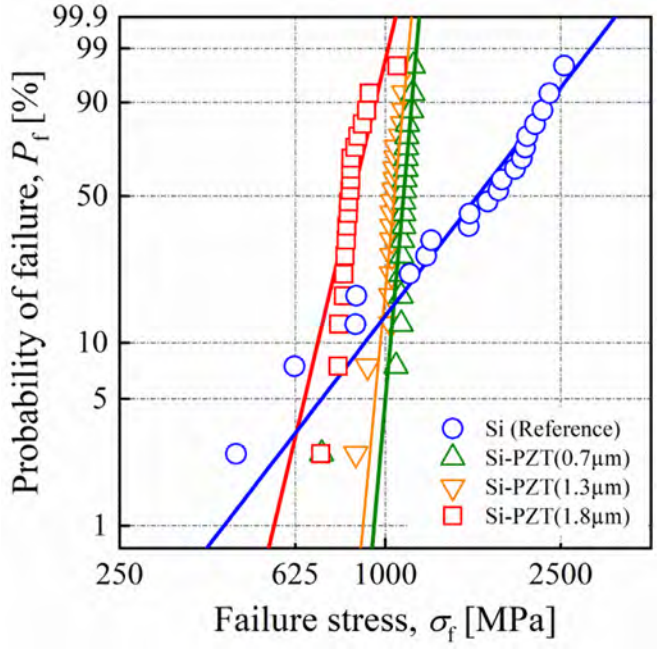

Fig. 3. The Weibull plot for the following samples: Si (blue circle), 1.8 μm PZT on Si (red square), 1.3 μm PZT on Si (orange downwards triangle), and 0.7 μm PZT on Si (green upwards triangle). The Weibull strength and Weibull modulus varied with the thickness of the PZT film on the Si wafer. (For interpretation of the references to colour in this figure legend, the reader is referred to the web version of this article.)

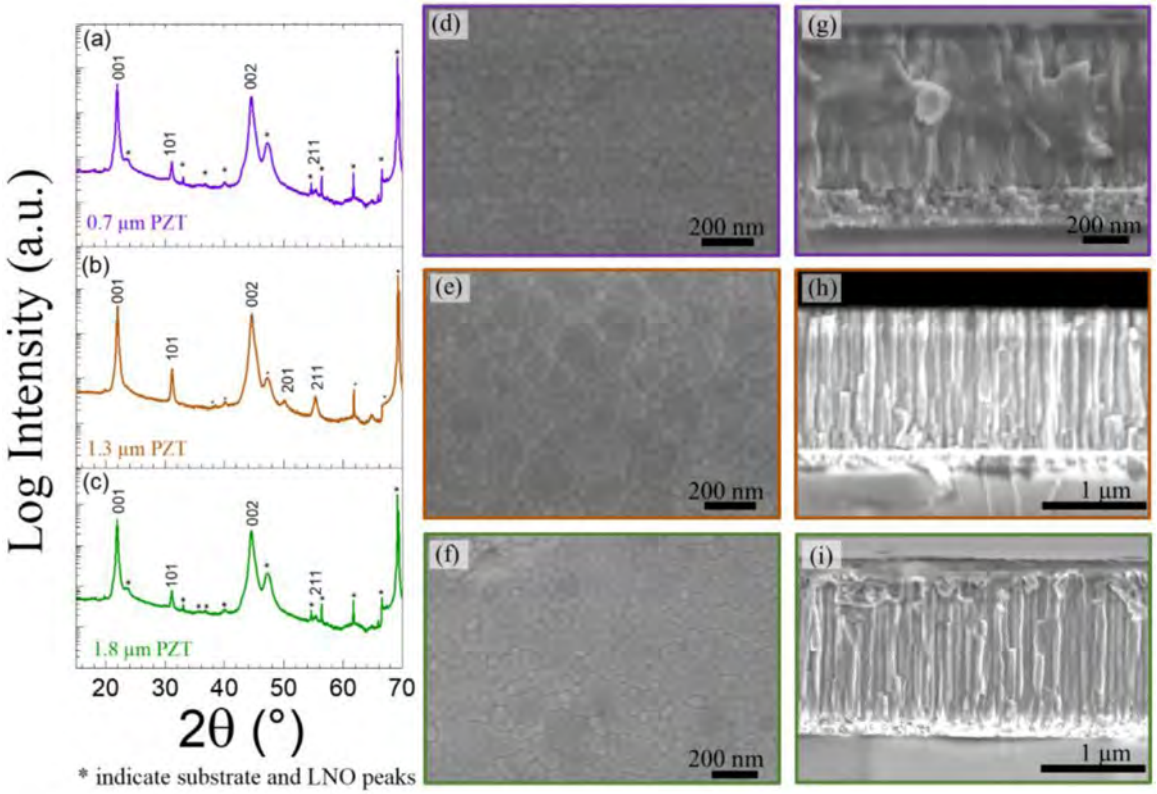

Fig. 2. XRD pattern of the 0.7 μm PZT (a), 1.3 μm PZT (b), and 1.8 μm PZT on Si (c), where the Lotgering factor is above 0.96 for all samples. The microstructure top view and cross section of the 0.7 μm (d and g respectively), 1.3 μm (e and h respectively), and 1.8 μm PZT sample (f and i respectively). The average grain size (diameter) of the 0.7 μm, 1.3 μm and 1.8 μm PZT film is 86 $\pm$ 7 nm, 105 $\pm$ 20 nm and 106 $\pm$ 14 nm, respectively.

Table 1
Characteristic load, characteristic strength, and Weibull modulus for the PZT/Si stacks of various thicknesses and the Si substrate. All stress values are in MPa and are calculated for the stress in the Si layer upon failure. Brackets represent 90% confidence intervals.

Sample	Characteristic Load, F_0 (N)	Characteristic Strength, σ_0 (MPa)	Weibull Modulus, m (-)
Si	190 [165 – 216]	1815 [1588 – 2081]	3 [2 – 4]
Si- 0.7 μm PZT	116 [114 – 117]	1114 [1097 – 1131]	28 [19 – 35]
Si- 1.3 μm PZT	111 [109 – 112]	1063 [1047 – 1082]	26 [18 – 33]
Si- 1.8 μm PZT	92 [87 – 95]	875 [839 – 912]	10 [7 – 13]

with thicker PZT layers, i.e. σ_0 = 1114 MPa for the 0.7 μm thin PZT film, σ_0 = 1063 MPa for the 1.3 μm film, and σ_0 = 875 MPa for the 1.8 μm film. Moreover, the stacks with the PZT layer have higher Weibull moduli than the Si substrate itself, suggesting failure from a narrower distribution of critical flaw sizes in the former.

3.3. Crack initiation

For the PZT films of 0.7 μm, 1.3 μm, and 1.8 μm the total force required to crack the PZT layer was (i) 64 N and higher for the 0.7 μm film, (ii) 56 N and higher for the 1.3 μm film, and (iii) 49 N and higher for the 1.8 μm films. The stress in the PZT layer was determined from Eq. (1) and adjusted for differences in the Young's modulus of PZT and Si (see supplementary section), corresponding to 590 $\pm$ 29 MPa, 540 $\pm$ 29 MPa, and 480 $\pm$ 29 MPa, for the 0.7, 1.3, and 1.8 μm films, respectively. The total stress in the PZT layer was calculated by adding 150 MPa of tensile residual stress in the PZT [35,43,44], which was measured by the wafer curvature method, to the applied stress [32]. The initial cracks did not cause fracture of the stack, which was still intact upon unloading. These initial cracks were only visible on the PZT side and were concentrated near the center of the sample, where the maximum tensile stress was applied, see supplemental information for optical images.

3.4. Crack propagation

Focused ion beam (FIB) cross sections of pre-loaded samples were used to determine the crack path during the biaxial bending tests. Fig. 4 shows a cross section of a crack propagating through the thickness of both the PZT and the LNO layers and arresting in the SiO_2 layer. Although the exact penetration depth of the crack into the SiO_2 layer could not be discerned due to "curtain effects" during FIB cross-section preparation, it is expected that the crack enters the SiO_2 layer and stops, as has been reported in literature for ceramic-ceramic multilayer architectures designed with compressive residual stresses [45].

4. Discussion

4.1. Residual stresses and Weibull volume effect

The stress required to initiate a crack in the PZT/LNO layers depends on the thickness of the PZT film. Thinner films require higher total stresses for crack initiation than do either thicker films or bulk PZT ceramics [46]. The experimental residual stresses are reported to be constant for PZT films above 350 nm thickness [10], which is consistent with calculations, see the supplemental materials. Therefore, it is unlikely that the differences in crack initiation stress between samples can be accounted for by a difference in the residual stress.

Another hypothesis is related to the Weibull volume effect [31]: larger material volumes loaded under the same applied tensile stress have higher probability of failure than smaller volumes in Weibull materials. That is, the characteristic strength, σ_i, of a sample with volume V_i, can be calculated based on the characteristic strength, σ_0, measured on a reference volume V_0, and the Weibull modulus of the material, m, according to [31,47]:

$$\sigma_i = \sigma_o \left(\frac{V_o}{V_i}\right)^{\frac{1}{m}} \tag{2}$$

In this work, the probability of failure from a critical flaw in samples with thinner PZT films should be lower.

To assess whether the volume dependence may account for the observed thickness dependence in the strength of the PZT samples, Eq. (2) was evaluated for different Weibull moduli, ranging from

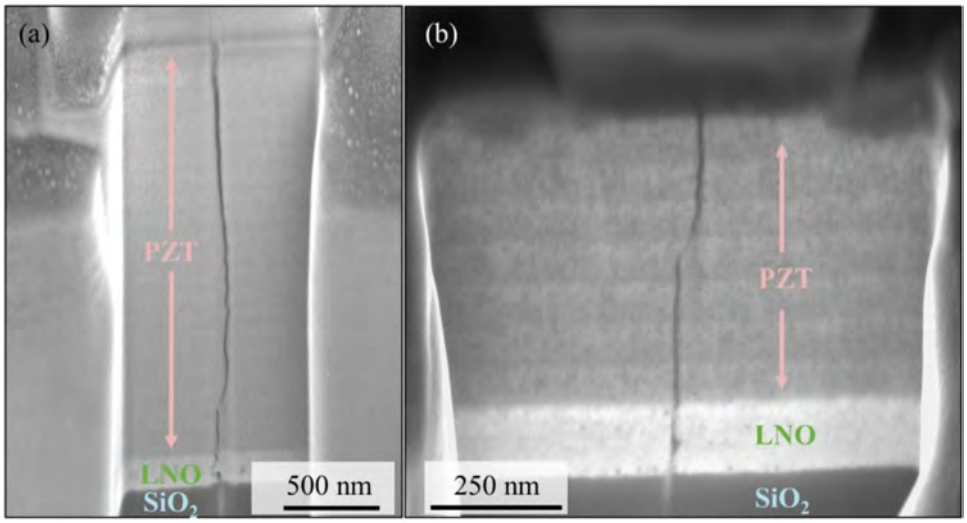

Fig. 4. FIB cross section of the (a) 1.8 μm PZT film's initial cracking and (b) the 0.7 μm PZT film's initial cracking. The crack propagates through the PZT layer and the LNO and ends at the SiO_2 layer. Initial cracks through the PZT and LNO layer were observed on multiple samples of varying stresses and PZT thicknesses. The faint line below the crack at the SiO_2 layer is an artifact of the FIB preparation.

m = 5 to m = 30, using the 0.7 μm PZT samples as a reference. Fig. 5 illustrates the volume effect on the predicted stress according to Eq. (3). The characteristic strength values for the three samples, i.e. (i) 0.7 μm, (ii) 1.3 μm, and (iii) 1.8 μm PZT film thickness samples are represented in Fig. 5 as full symbols. The volume ratio V_0/V_i was set equal to the thickness ratio. According to the results in Fig. 5, the volume effect may explain the differences in crack initiation stresses between two samples, provided that the Weibull modulus of the PZT material is $m \sim 5$. In this regard, based on the homogeneous microstructure of the PZT films and the relatively narrow crack initiation stress values obtained in all three samples, a Weibull modulus larger than 15 is expected [40]; this higher value also corresponds with Weibull modulus for bulk PZT ceramics [48]. This suggests that the volume effect alone cannot explain the differences in crack initiation stress.

4.2. Model for crack initiation

Linear Elastic Fracture Mechanics can only describe the conditions for crack propagation assuming that an initial crack already exists. To predict crack initiation, the classical (Griffith-Irwin) criterion for crack propagation is insufficient, and a different approach must be considered. Finite Fracture Mechanics (FFM) states that under applied mechanical stress, a crack initiates having a "finite" length (in many cases of the order of the microstructure) when certain stress and energy conditions are satisfied [49]. FFM utilizes a stress-energy coupled criterion (referred to as CC), where a crack originates if two conditions (i.e. stress and energy conditions) are simultaneously fulfilled – namely $\sigma(a) \geq \sigma_c$ and $G_{inc}(a) \geq G_c$ where σ is the stress at the site of the potential crack, G_{inc} is the increment of the potential energy for finite crack length increments, and σ_c and G_c are the material's strength and toughness, respectively. The first condition states that the normal tensile stress should be higher than the material tensile strength along the entire potential crack path, and the second condition stipulates that there should be enough energy available to create that crack [50]. This criterion has explained the onset of cracks in thin polymer films on substrates [32] or the generation of surface edge cracks in layered ceramics [51]. In both cases, the potential energy during loading increases with the thickness of the layer containing the prospective crack. As a result, under the same loading conditions and properties, cracks can initiate in thicker layers under smaller applied loads.

In order to assess the crack initiation stress condition in the three PZT samples of study a material biaxial strength of $\sigma_c \approx 200$ MPa was assumed for the PZT layer, based on the values reported in literature for bulk PZT [46,48,52]. A range of fracture toughness for PZT bulk ceramics has been reported between 0.6 and 1.8 MPa$\sqrt{m}$ [53–56] and these differences have been attributed to domain mobility, where toughness increases with the increasing levels of domain wall motion [55]. In this model, since the films are clamped to the substrate and clamping lowers domain wall mobility [5,6], low values of K_{Ic} (0.6 to 1 MPa$\sqrt{m}$) were used in the calculations. In addition, a homogeneous stress distribution in the sample during B3B was assumed. Fig. 6 represents the calculated crack initiation stress for different PZT thicknesses from 0.6 μm to 2.0 μm and K_{Ic} values of 0.6, 0.8, and 1 MPa$\sqrt{m}$. The full symbols represent the crack initiation stress measured in the pre-loading B3B experiment.

According to the results in Fig. 6, samples with thinner PZT layers require higher stresses to initiate cracks. The calculations for the case of thicker PZT with K_{Ic} = 0.6 MPa$\sqrt{m}$ fit well the observed crack initiation stress values from the B3B experiments. However, the stress predicted for the thinner films overestimates the experimental data. The errors in the calculated values are likely to be due to the use of a constant K_{Ic} value, as noted above, the value of K_{Ic} depends on domain wall motion [53,55,57]. Since thicker films generally exhibit more domain wall motion and ferroelastic switching [5,6], K_{Ic} may be a function of thickness. As a result, the energy criteria should have a shallower slope, which would better match the observed trend. More quantitative comparisons would require direct measurements of both K_{Ic} and the ferroelastic switching as a function of the applied stress and the PZT layer thickness. It is worth mentioning that the levels of crack initiation stress (i.e. $\sim$ 500 – 600 MPa) in this study (both predicted and measured) are much higher than the strength of bulk PZT, σ_c, measured in similar biaxial configurations (i.e. $\sim$ 100 – 200 MPa) [48,58]. This shows evidence that the energy criterion is also needed to describe the initiation of cracks in brittle ferroelectric

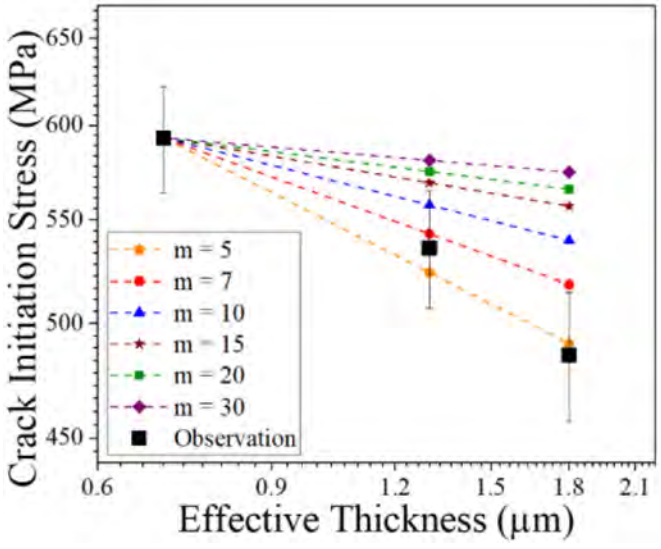

Fig. 5. Calculated relationship between crack initiation stress and the thickness of the PZT layer using the Weibull volume effect compared to the experimental data. Black squares represent the characteristic crack initiation stress, and the dashed lines are calculated, using the crack initiation stress of the 0.7 μm thick PZT layer as a reference. The various colors represent estimations using different Weibull moduli for PZT for each calculation. (For interpretation of the references to colour in this figure legend, the reader is referred to the web version of this article.)

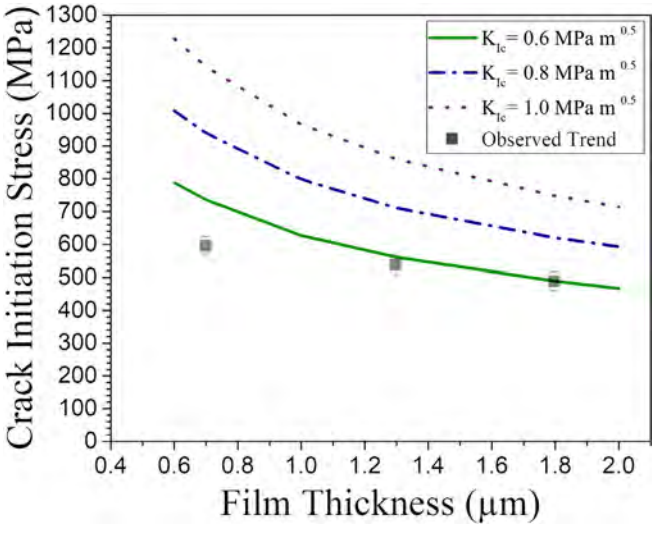

Fig. 6. Comparison of the strength as a function of thickness for the observed trends (gray squares), and finite fracture mechanics model predictions (K_{Ic}=0.6, K_{Ic}=0.8, and K_{Ic}=1.0, are the green solid line, blue dot-dash line, and purple dotted line, respectively). The observation of this thickness dependence follows the finite fracture mechanics model for thicknesses larger than 1 μm, however it fails for very thin films. This may be due to domain wall contributions which are not taken into account in the model. (For interpretation of the references to colour in this figure legend, the reader is referred to the web version of this article.)

materials, and is particularly important in multilayer systems as the one in this study.

4.3. Model for crack propagation

Based on the experimental observations (Fig. 4), crack initiation in the PZT film is followed by crack propagation and arrest at the SiO_2 layer. This occurs in the 0.7 μm, 1.3 μm, and 1.8 μm PZT film samples of study. Crack arrest in the SiO_2 may be explained either by a significant change in the crack growth resistance of the material as the crack advances (referred to as R-curve behavior) or due to shielding effects associated with compressive residual stresses in the layer. The former does not apply, because the fracture toughness of SiO_2 does not change with the crack length, and has been reported to be $\sim$ 0.85 MPa$\sqrt{m}$ [29]. The presence of compressive residual stresses however may hinder crack propagation, depending on the magnitude of stress and layer thickness, as has been demonstrated for instance in layered ceramics [45]. The conditions for crack propagation compare the stress intensity factor at the crack tip during loading with the crack growth resistance in the particular layer where the tip of the crack is located. The stress intensity factor at the crack tip is a function of the crack length, $K_{tip}(a)$, and can be given as the externally applied stress intensity factor $K_{appl}(a)$ plus the contribution of the residual stresses, as shown in Eq. (3). Note the film is under plane stress conditions and substrate bending is negligible.

$$K_{tip}(a) = K_{appl}(a) + K_{res}(a) \tag{3}$$

$K_{appl}(a)$ can be calculated according to Griffith criterion based on Linear Elastic Fracture Mechanics, where [59,60]:

$$K_{appl}(a) = \sigma_{appl} Y \sqrt{a} \tag{4}$$

with σ_{appl} being the stress applied during loading. The term $K_{res}(a)$ represents the residual stress intensity factor as a function of the position of the crack tip within the corresponding layer in the stack. In order to account for the contribution of residual stresses through the multilayer stack, a weight function analysis may be employed [45]. The weighting function is related to the crack geometry (e.g. through-thickness crack, wedged crack, etc.) and loading condition (e.g. three-point or four-point bending) [61]. In this analysis, the residual stresses profile in each layer is "weighted" along the corresponding layer thickness. The differences in elastic constants between layers are not considered in the analysis. However, when the elastic mismatch between the layers is less than a factor of 10, the change in the stress intensity factor estimation is negligible [62]. Solving Eq. (3) for K_{appl}, the Griffith/Irwin criterion described in Eq. (4) becomes:

$$K_{appl(a)} \geq K_{Ic(a)} - K_{res(a)} = K_{R(a)} \tag{5}$$

where $K_R(a)$ is defined as the "apparent fracture toughness" of the layered ceramic.

Fig. 7 represents K_R for the three types of samples as a function of the crack length parameter $Y(a)^{1/2}$ (defined to simplify the analysis), with Y being the geometric factor that accounts for the crack shape and loading configuration. The material parameters including the mechanical properties and thermal expansion coefficients of the various layers for this estimation of the residual stresses in each layer and the calculation of K_{res} are listed in the supplemental information [8,44,63–67]. In this case, Y can be taken as for a central penny-shaped crack at the surface (i.e. $Y = 2 / \sqrt{\pi} \approx 1.12$) [68]. The applied stress intensity factor, $K_{appl}(a)$, is represented in Fig. 7 (as dashed lines). According to Eq. (4), the slope of those dashed lines represents the applied stress, σ_{appl}. The analysis has been performed for a symmetric stack, thus neglecting the slight bending due to the asymmetric architecture.

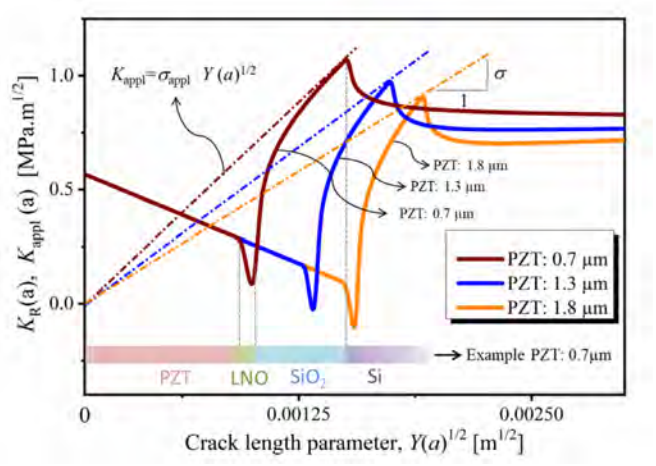

Fig. 7. Apparent toughness of the multilayer stack as a function of the crack length and the residual stress, and thickness of the various layers.

The three curves in Fig. 7 represent the crack growth resistance through the three multilayers of this study, taking into account the residual stresses in the layers. The dashed lines represent the applied stress intensity factor as a function of the crack length $K_{appl}(a)$, for a particular applied stress, σ_{appl} (i.e. the slope of the dashed line). It is clear that the crack growth resistance decreases as the crack enters in the PZT layer. This is a consequence of the in-plane tensile stress in that layer; the same situation applies for the LNO layer (see supplemental information). However, due to the compressive residual stress in the SiO_2 layer, a rising crack growth resistance is observed, thus shielding the propagation of the crack. This "R-curve behavior" is similar in the three architectures; however, the anti-shielding effect of the first layer is related to the PZT film thickness. As a consequence, the minimum stress necessary to propagate the crack through the stack is higher for the 0.7 μm thick PZT layer than in the other two. This agrees with the B3B experimental measurements.

This investigation demonstrates that stack failure occurs in two stages. A relatively modest stress ($\sim$500 – 600 MPa) cracks the PZT and LNO layers [22]. The initial crack acts as a critical flaw for the failure of the SiO_2/Si substrate. As the initial cracks are of consistent length (the sum of the PZT and LNO thicknesses) and the fracture toughness of SiO_2 is constant, the stack fails at a relative similar stress level for a given PZT thickness. This, in turn, produces the higher Weibull modulus of the PZT stack relative to the SiO_2/Si substrate itself. This model also accounts for the observation that the Weibull characteristic strength drops as the PZT thickness increases. That is, thinner PZT layers display shorter initial crack lengths and require higher stresses to propagate the crack through the SiO_2 layer.

5. Conclusions

This study demonstrates that the thickness of PZT films employed in PiezoMEMS has a significant influence on the crack onset and fracture resistance of the entire stack. Biaxial strength measurements on stacks containing different PZT layers grown on $\sim$500 μm Si substrates showed a decrease in the characteristic strength, σ_0, with the PZT layer thickness, ranging from $\sigma_0 \sim$ 1110 MPa for 0.7 μm thin film stacks, to $\sigma_0 \sim$ 1060 MPa for the 1.3 μm thin film stack, and $\sigma_0 \sim$ 880 MPa for the 1.8 μm film stack. These values were significantly lower than the strength of the Si substrate, i.e. $\sigma_0 \sim$ 1820 MPa. The higher Weibull modulus obtained in the PZT-Si stacks (i.e. $m \sim 28$ for the 0.7 μm thin film stack, $m \sim 26$ for the 1.3 μm thin film stack, and $m \sim 10$ for the 1.8 μm film stack) compared to Si substrate (i.e. $m \sim 3$) indicated that the PZT/LNO layer thickness becomes the critical flaw size for failure of the entire stack. A stress-energy criterion based

on finite fracture mechanics was employed to explain the higher applied load necessary to initiate cracks in the stack containing a thinner PZT layer. Biaxial tests to pre-crack the stacks showed the same trend as the model. This coupled criterion for crack initiation may be extended to complex ferroic materials, if the domain responses are taken into account. Indeed, this could ultimately become a method to quantitatively understand domain wall mobility in ferroic structures under stress. In addition, observation of crack arrest within the multilayer structure prior to the fracture of the entire stack suggests the possibility of tailoring the internal architecture (such as adding compressive layers, or changing the residual stress in the film) of PiezoMEMS to enhance mechanical integrity and thus performance.

Declaration of Competing Interest

The authors declare that they have no known competing financial interests or personal relationships that could have appeared to influence the work reported in this paper.

Acknowledgment

This manuscript is based on work supported by the National Science Foundation, as part of the Center for Dielectrics and Piezoelectrics under Grant Nos. IIP-1361571, IIP-1361503, IIP-1841453, and IIP-1841466.

The authors would like to acknowledge Robert Danzer, Peter Supancic, Josef Kreith from the Lehrstuhl fuer Struktur- und Funktionskeramik, Montanuniversitaet Leoben, Austria, for fruitful discussions on the stress analysis and Weibull evaluation. The authors would also like to acknowledge Trevor Clark at the Materials Characterization Lab at Penn State for the FIB images.

Supplementary materials

Supplementary material associated with this article can be found in the online version at doi:10.1016/j.actamat.2020.03.030.

References

[1] P. Muralt, R.G. Polcawich, S. Trolier-McKinstry, Piezoelectric thin films for sensors, actuators, and energy harvesting, MRS Bull. 34 (2009) 658–664, doi: 10.1557/mrs2009.177.

[2] N. Izyumskaya, Y.I. Alivov, S.J. Cho, H. Morkoç, H. Lee, Y.S. Kang, Processing, structure, properties, and applications of PZT thin films, Crit. Rev. Solid State Mater. Sci. 32 (2007) 111–202, doi: 10.1080/10408430701707347.

[3] D. Damjanovic, Ferroelectric, dielectric and piezoelectric properties of ferroelectric thin films and ceramics, Rep. Prog. Phys. 61 (1998) 1267–1324, doi: 10.1088/0034-4885/61/9/002.

[4] H.G. Yeo, X. Ma, C. Rahn, S. Trolier-McKinstry, Efficient piezoelectric energy harvesters utilizing (001) textured bimorph PZT films on flexible metal foils, Adv. Funct. Mater. 26 (2016) 5940–5946, doi: 10.1002/adfm.201601347.

[5] L.M. Denis, G. Esteves, J. Walker, J.L. Jones, S. Trolier-McKinstry, Thickness dependent response of domain wall motion in declamped {001} $Pb(Zr_{0.3}Ti_{0.7})O_3$ thin films, Acta Mater. 151 (2018) 243–252, doi: 10.1016/j.actamat.2018.03.046.

[6] G. Han, J. Ryu, W.H. Yoon, J.J. Choi, B.D. Hahn, D.S. Park, Effect of film thickness on the piezoelectric properties of lead zirconate titanate thick films fabricated by aerosol deposition, J. Am. Ceram. Soc. 94 (2011) 1509–1513, doi: 10.1111/j.1551-2916.2010.04276.x.

[7] C.B. Yeager, S. Trolier-McKinstry, Epitaxial $Pb(Zr_x,Ti_{1-x})O_3$ ($0.30 \leq x \leq 0.63$) films on (100) MgO substrates for energy harvesting applications, J. Appl. Phys. 112 (2012) 074107, doi: 10.1063/1.4754015.

[8] B.A. Tuttle, J.A. Voigt, T.J. Garino, D.C. Goodnow, R.W. Schwartz, D.L. Lamppa, T.J. Headley, M.O. Eatough, Chemically prepared $Pb(Zr,Ti)O_3$ thin films: the effects of orientation and stress, ISAF '92 Proceedings of the Eighth IEEE International Symposium on Applications of Ferroelectrics, 1992, pp. 344–348, doi: 10.1109/ISAF.1992.300703.

[9] R.J. Ong, D.A. Payne, N.R. Sottos, Processing effects for integrated PZT: residual stress, thickness, and dielectric properties, J. Am. Ceram. Soc. 88 (2005) 2839–2847, doi: 10.1111/j.1551-2916.2005.00641.x.

[10] T.A. Berfield, R.J. Ong, D.A. Payne, N.R. Sottos, Residual stress effects on piezoelectric response of sol-gel derived lead zirconate titanate thin films, J. Appl. Phys. 101 (2007) 024102, doi: 10.1063/1.2422778.

[11] M.D. Nguyen, M. Dekkers, E. Houwman, R. Steenwelle, X. Wan, A. Roelofs, T. Schmitz-Kempen, G. Rijnders, Misfit strain dependence of ferroelectric and piezoelectric properties of clamped (001) epitaxial $Pb(Zr_{0.52},Ti_{0.48})O_3$ thin films, Appl. Phys. Lett. 99 (2011) 252904, doi: 10.1063/1.3669527.

[12] R. Treml, D. Kozic, J. Zechner, X. Maeder, B. Sartory, H.P. Gänser, R. Schöngrundner, J. Michler, R. Brunner, D. Kiener, High resolution determination of local residual stress gradients in single- and multilayer thin film systems, Acta Mater. 103 (2016) 616–623, doi: 10.1016/j.actamat.2015.10.044.

[13] E. Chason, P.R. Guduru, Tutorial: understanding residual stress in polycrystalline thin films through real-time measurements and physical models, J. Appl. Phys. 119 (2016) 191101, doi: 10.1063/1.4949263.

[14] K. Nishida, M. Osada, S. Wada, S. Okamoto, R. Ueno, H. Funakubo, T. Katoda, A new method to characterize a relative volume to the c-domain in PZT films based on Raman spectra, Integr. Ferroelectr. 78 (2006) 281–287, doi: 10.1080/10584580600663425.

[15] G.A.C.M. Spierings, G.J.M. Dormans, W.G.J. Moors, M.J.E. Ulenaers, P.K. Larsen, Stresses in $Pt/Pb(Zr,Ti)O_3/Pt$ thin-film stacks for integrated ferroelectric capacitors, J. Appl. Phys. 78 (1995) 1926–1933, doi: 10.1063/1.360230.

[16] C.B. Yeager, Y. Ehara, N. Oshima, H. Funakubo, S. Trolier-McKinstry, Dependence of $e_{31,f}$ on polar axis texture for tetragonal $Pb(Zr_x,Ti_{1-x})O_3$ thin films, J. Appl. Phys. 116 (2014) 104907, doi: 10.1063/1.4895339.

[17] H.G. Yeo, S. Trolier-McKinstry, {001} oriented piezoelectric films prepared by chemical solution deposition on Ni foils, J. Appl. Phys. 116 (2014) 014105, doi: 10.1063/1.4886597.

[18] H.D. Chen, K. Udayakumar, K.K. Li, C.J. Gaskey, L.E. Cross, Dielectric breakdown strength in sol-gel derived PZT thick films, Integr. Ferroelectr. 15 (1997) 89–98, doi: 10.1080/10584589708015699.

[19] W. Zhu, T. Borman, K. Decesaris, B. Truong, M.M. Lieu, S.W. Ko, P. Mardilovich, S. Trolier-McKinstry, Influence of PbO content on the dielectric failure of Nb – doped {100} – oriented lead zirconate titanate films, J. Am. Ceram. Soc. 102 (2018) 1–7, doi: 10.1111/jace.16000.

[20] T.M. Borman, W. Zhu, K. Wang, S.W. Ko, P. Mardilovich, S.E. Trolier-McKinstry, Effect of lead content on the performance of niobium-doped {100} textured lead zirconate titanate films, J. Am. Ceram. Soc. (2017) 3558–3567, doi: 10.1111/jace.14892.

[21] Z. Luo, S. Pojprapai, J. Glaum, M. Hoffman, Electrical fatigue-induced cracking in lead zirconate titanate piezoelectric ceramic and its influence quantitatively analyzed by refatigue method, J. Am. Ceram. Soc. 95 (2012) 2593–2600, doi: 10.1111/j.1551-2916.2012.05232.x.

[22] A. Mazzalai, D. Balma, N. Chidambaram, P. Muralt, L. Colombo, T. Schmitz-Kempen, Dynamic and long-time tests of the transverse piezoelectric coefficient in PZT thin films, in: Proceedings of the Joint IEEE International Symposium on the Applications of Ferroelectric, International Workshop on Acoustic Transduction Materials and Devices & Workshop on Piezoresponse Force Microscopy ISAF/IWATMD/PFM 2014, 2014, doi: 10.1109/ISAF.2014.6922998.

[23] M.A. Dubois, P. Muralt, Measurement of the effective transverse piezoelectric coefficient $e_{31,f}$ of AlN and $Pb(Zr_x,Ti_{1-x})O_3$ thin films, Sens. Actuat. A Phys 77 (1999) 106–112, doi: 10.1016/S0924-4247(99)00070-9.

[24] J.F. Shepard, S. Trolier-McKinstry, M.A. Hendrickson, R. Zeto, Properties of PZT thin films as a function of in-plane biaxial stress, ISAF '96. Proceedings of the Tenth IEEE International Symposium on Applications of Ferroelectrics, 1, 1996, pp. 161–165, doi: 10.1109/ISAF.1996.602728.

[25] S. Trolier-McKinstry, C.A. Randall, J.P. Maria, C. Theis, D.G. Schlom, J. Shepard, K. Yamakawa, Size effects and domains in ferroelectric thin film actuators, MRS Proc. 433 (1996) 363–374, doi: 10.1557/PROC-433-363.

[26] D. Damjanovic, F. Chu, D.V. Taylor, M.D. Maeder, L. Sagalowicz, P.D. Martin, N. Setter, Engineering of piezoelectric properties in ferroelectric, Cerám. Vidr. 38 (1999) 538–544.

[27] K.S. Chen, A. Ayon, S.M. Spearing, Controlling and testing the fracture strength of silicon on the mesoscale, J. Am. Ceram. Soc. 83 (2000) 1476–1484, doi: 10.1111/j.1151-2916.2000.tb01413.x.

[28] C. Funke, E. Kullig, M. Kuna, H.J. Möller, Biaxial fracture test of silicon wafers, Adv. Eng. Mater. 6 (2004) 594–598, doi: 10.1002/adem.200400406.

[29] D.H. Alsem, B.L. Boyce, E.A. Stach, R.O. Ritchie, Effect of post-release sidewall morphology on the fracture and fatigue properties of polycrystalline silicon structural films, Sens. Actuat. A Phys. 147 (2008) 553–560, doi: 10.1016/j.sna.2008.05.027.

[30] O.M. Jadaan, N.N. Nemeth, J. Bagdahn, W.N. Sharpe, Probabilistic Weibull behavior and mechanical properties of MEMS brittle materials, J. Mater. Sci. 38 (2003) 4087–4113, doi: 10.1023/A:1026317303377.

[31] W. Weibull, A Statistical Theory of Strength of Materials, Royal Swedish Institute for Engineering Research, 1939.

[32] D. Leguillon, E. Martin, Prediction of multi-cracking in sub-micron films using the coupled criterion, Int. J. Fract. 209 (2018) 187–202, doi: 10.1007/s10704-017-0255-6.

[33] H. Nagata, S.W. Ko, E. Hong, C.A. Randall, S. Trolier-McKinstry, P. Pinceloup, D. Skamser, M. Randall, A. Tajuddin, Microcontact printed $BaTiO_3$ and $LaNiO_3$ thin films for capacitors, J. Am. Ceram. Soc. 89 (2006) 2816–2821, doi: 10.1111/j.1551-2916.2006.01137.x.

[34] T. Tani, D.A. Payne, Lead oxide coatings on sol-gel-derived lead lanthanum zirconium titanate thin layers for enhanced crystallization into the perovskite structure, J. Am. Ceram. Soc. 77 (1994) 1242–1248.

[35] K. Coleman, J. Walker, T. Beechem, S. Trolier-McKinstry, Effects of stresses on the dielectric and piezoelectric properties of $Pb(Zr_{0.52}Ti_{0.48})O_3$ thin films, J. Appl. Phys. 126 (2019) 034101, doi: 10.1063/1.5095765.

[36] A. Börger, P. Supancic, R. Danzer, The ball on three balls test for strength testing of brittle discs: part II: analysis of possible errors in the strength determination, J. Eur. Ceram. Soc. 24 (2004) 2917–2928, doi: 10.1016/j.jeurceramsoc.2003.10.035.

[37] R. Danzer, P. Supancic, W. Harrer, Biaxial tensile strength test for brittle rectangular plates, J. Ceram. Soc. Jpn. 114 (2006) 1054–1060, doi: 10.2109/jcersj.114.1054.
[38] M. Deluca, R. Bermejo, M. Pletz, P. Supancic, R. Danzer, Strength and fracture analysis of silicon-based components for embedding, J. Eur. Ceram. Soc. 31 (2011) 549–558, doi: 10.1016/j.jeurceramsoc.2010.10.029.
[39] M. Deluca, R. Bermejo, M. Pletz, M. Wießner, P. Supancic, R. Danzer, Influence of deposited metal structures on the failure mechanisms of silicon-based components, J. Eur. Ceram. Soc. 32 (2012) 4371–4380, doi: 10.1016/j.jeurceramsoc.2012.06.027.
[40] R. Bermejo, P. Supancic, R. Danzer, Influence of measurement uncertainties on the determination of the Weibull distribution, J. Eur. Ceram. Soc. 32 (2012) 251–255, doi: 10.1016/j.jeurceramsoc.2011.09.008.
[41] ASTM C1239-13(2018), Standard practice for reporting uniaxial strength data and estimating Weibull distribution parameters for advanced ceramics, ASTM International, West Conshohocken, PA, 2018. n.d.
[42] T. Yi, L. Li, C.-J. Kim, Microscale material testing of single crystalline silicon: process effects on surface morphology and tensile strength, Sens. Actuat. A Phys. 83 (2000) 172–178, doi: 10.1016/S0924-4247(00)00350-2.
[43] I. Chasiotis, W.G. Knauss, The mechanical strength of polysilicon films: part 1. The influence of fabrication governed surface conditions, J. Mech. Phys. Solids 51 (2003) 1533–1550, doi: 10.1016/S0022-5096(03)00051-6.
[44] D. Das, L. Sanchez, J. Martin, B. Power, S. Isaacson, R.G. Polcawich, I. Chasiotis, Control of mechanical response of freestanding $PbZr_{0.52}Ti_{0.48}O_3$ films through texture, Appl. Phys. Lett. 109 (2016) 131905, doi: 10.1063/1.4963348.
[45] R. Bermejo, "Toward seashells under stress": bioinspired concepts to design tough layered ceramic composites, J. Eur. Ceram. Soc. 37 (2017) 3823–3839, doi: 10.1016/j.jeurceramsoc.2017.04.041.
[46] L. Hai-Bo, C. Mao-Sheng, Y. Jie, W. Da-Wei, Z. Quan-Liang, W. Fu-Chi, Enhanced mechanical behaviour of lead zirconate titanate piezoelectric composites incorporating zinc oxide nanowhiskers, Chin. Phys. B. 17 (2008) 4323–4327.
[47] W. Weibull, A statistical distribution function of wide applicability, J. Appl. Mech. (1951) 293–297.
[48] K. Zhang, F.W. Zeng, H. Wang, H.T. Lin, Biaxial flexural strength of poled lead zirconate titanate under high electric field with extended field range, Ceram. Int. 39 (2013) 2023–2030, doi: 10.1016/j.ceramint.2012.08.054.
[49] D. Taylor, The theory of critical distances, Eng. Fract. Mech. 75 (2008) 1696–1705, doi: 10.1016/j.engfracmech.2007.04.007.
[50] D. Leguillon, Strength or toughness? A criterion for crack onset at a notch, Eur. J. Mech. A Solids 21 (2002) 61–72, doi: 10.1016/S0997-7538(01)01184-6.
[51] O. Ševeček, M. Kotoul, D. Leguillon, E. Martin, R. Bermejo, Modelling of edge crack formation and propagation in ceramic laminates using the stress–energy coupled criterion, Eng. Fract. Mech. 167 (2016) 45–55, doi: 10.1016/j.engfracmech.2016.03.039.
[52] P. Supancic, Z. Wang, W. Harrer, K. Reichmann, R. Danzer, Strength and fractorgraphy of piezoceramics multilayer stacks, Key Eng. Mater. 290 (2005) 46–53.
[53] Y.H. Seo, A. Benčan, J. Koruza, B. Malič, M. Kosec, K.G. Webber, Compositional dependence of R-curve behavior in soft $Pb(Zr_{1-x}Ti_x)O_3$ ceramics, J. Am. Ceram. Soc. 94 (2011) 4419–4425, doi: 10.1111/j.1551-2916.2011.04889.x.
[54] S.L. dos Santos e Lucato, D.C. Lupascu, J. Rödel, Effect of poling direction on R-curve behavior in lead zirconate titanate, J. Am. Ceram. Soc. 83 (2000) 424–426, doi: 10.1111/j.1151-2916.2000.tb01210.x.
[55] K. Mehta, A.V. Virkar, Fracture mechanisms in ferroelectric–ferroelastic lead zirconate titanate (Zr: Ti=0.54:0.46) ceramics, J. Am. Ceram. Soc. 73 (1990) 567–574, doi: 10.1111/j.1151-2916.1990.tb06554.x.
[56] R. Bermejo, H. Grünbichler, J. Kreith, C. Auer, Fracture resistance of a doped PZT ceramic for multilayer piezoelectric actuators: effect of mechanical load and temperature, J. Eur. Ceram. Soc. 30 (2010) 705–712, doi: 10.1016/j.jeurceramsoc.2009.08.013.
[57] R.J. Zednik, A. Varatharajan, M. Oliver, N. Valanoor, P.C. McIntyre, Mobile ferroelastic domain walls in nanocrystalline PZT films: the direct piezoelectric effect, Adv. Funct. Mater. 21 (2011) 3104–3110, doi: 10.1002/adfm.201100445.
[58] H. Wang, A. Wereszczak, Effects of electric field on the biaxial strength of poled PZT, Adv. Electron. Ceram. (2008) 57–67.
[59] A.A. Griffith, The phenomena of rupture and flow in solids, Philosophical Transactions of the Royal Society of London, Sereis A. Vol. 221 (1921) 163–198.
[60] G.R. Irwin, Linear fracture mechanics, fracture transition, and fracture control, Eng. Fract. Mech. 1 (1968) 241–257.
[61] T. Fett, D. Munz, Stress intensity factor and weight functions, Southampton (1997), doi: 10.5860/choice.35-2724.
[62] L. Sestakova, R. Bermejo, Z. Chlup, R. Danzer, Strategies for fracture toughness, strength and reliability optimisation of ceramic – ceramic laminates, Int. J. Mater. Research. 102 (2011) 1–14.
[63] G.C.A.M. Janssen, M.M. Abdalla, F. van Keulen, B.R. Pujada, B. van Venrooy, Celebrating the 100th anniversary of the Stoney equation for film stress: developments from polycrystalline steel strips to single crystal silicon wafers, Thin Solid Films 517 (2009) 1858–1867, doi: 10.1016/j.tsf.2008.07.014.
[64] W.R. Cook, D.A. Berlincourt, F.J. Scholz, Thermal expansion and pyroelectricity in lead titanate zirconate and barium titanate, J. Appl. Phys. 34 (1963) 1392–1398, doi: 10.1063/1.1729587.
[65] Y. Okada, Y. Tokumaru, Precise determination of lattice parameter and thermal expansion coefficient of silicon between 300 and 1500K, J. Appl. Phys. 56 (1984) 314–320, doi: 10.1063/1.333965.
[66] Y. Tsuru, M. Shimazu, M. Shiono, M. Morinaga, Evaluation of linear thermal expansion coefficients of perovskite oxides using ab-initio molecular dynamics with small cell sizes for materials design, Jpn. J. Appl. Phys. 49 (2010) 0457011–0457015, doi: 10.1143/JJAP.49.045701.
[67] S. Masys, V. Jonauskas, Elastic properties of rhombohedral, cubic, and monoclinic phases of $LaNiO_3$ by first principles calculations, Comput. Mater. Sci. 108 (2015) 153–159, doi: 10.1016/j.commatsci.2015.06.034.
[68] R.W. Hertzberg, R.P. Vinci, J.L. Hertzberg, Elements of Fracture Mechanics, Deformation and Fracture Mechanics of Engineering Materials, 5th Edition. 2012, pp. 299–381.